ACSNANO

www.acsnano.org

ARTICLE

Rapid Detection of COVID-19 Causative Virus (SARS-CoV-2) in Human Nasopharyngeal Swab Specimens Using Field-Effect Transistor-Based Biosensor

Giwan Seo, Geonhee Lee, Mi Jeong Kim, Seung-Hwa Baek, Minsuk Choi, Keun Bon Ku, Chang-Seop Lee, Sangmi Jun, Daeui Park, Hong Gi Kim, Seong-Jun Kim, Jeong-O Lee, Bum Tae Kim, Edmond Changkyun Park,* and Seung Il Kim*

Cite This: https://dx.doi.org/10.1021/acsnano.0c02823

Read Online

ACCESS | Metrics & More | Article Recommendations | Supporting Information

ABSTRACT: Coronavirus disease 2019 (COVID-19) is a newly emerging human infectious disease caused by severe acute respiratory syndrome coronavirus 2 (SARS-CoV-2, previously called 2019-nCoV). Based on the rapid increase in the rate of human infection, the World Health Organization (WHO) has classified the COVID-19 outbreak as a pandemic. Because no specific drugs or vaccines for COVID-19 are yet available, early diagnosis and management are crucial for containing the outbreak. Here, we report a field-effect transistor (FET)-based biosensing device for detecting SARS-CoV-2 in clinical samples. The sensor was produced by coating graphene sheets of the FET with a specific antibody against SARS-CoV-2 spike protein. The performance of the sensor was determined using antigen protein, cultured virus, and nasopharyngeal swab specimens from COVID-19 patients. Our FET device could detect the SARS-CoV-2 spike protein at concentrations of 1 fg/mL in phosphate-buffered saline and 100 fg/mL clinical transport medium. In addition, the FET sensor successfully detected SARS-CoV-2 in culture medium (limit of detection [LOD]: 1.6×10^1 pfu/mL) and clinical samples (LOD: 2.42×10^2 copies/mL). Thus, we have successfully fabricated a promising FET biosensor for SARS-CoV-2; our device is a highly sensitive immunological diagnostic method for COVID-19 that requires no sample pretreatment or labeling.

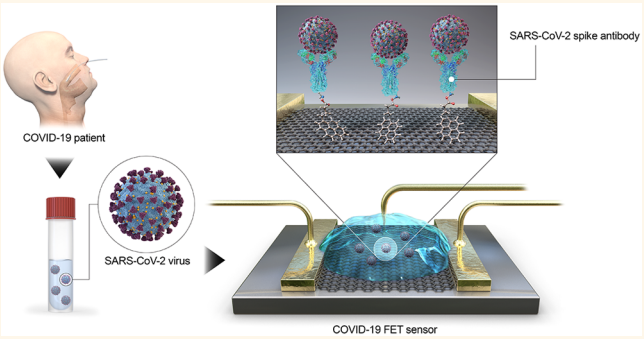

KEYWORDS: *FET, biosensor, COVID-19, SARS-CoV-2, 2019-nCoV*

Coronavirus disease 2019 (COVID-19) is a newly emerging human infectious disease associated with severe respiratory distress. In December 2019, a series of cases of pneumonia of unknown cause were reported in Wuhan in the Hubei province of China.[1] Later, the 2019 novel coronavirus (2019-nCov) was identified from the bronchoalveolar lavage fluid of a patient;[2] it was subsequently renamed severe acute respiratory syndrome coronavirus 2 (SARS-CoV-2) by the International Committee on Taxonomy of Viruses.[3] As human-to-human transmission rapidly increased, the World Health Organization (WHO) classified the COVID-19 outbreak as a pandemic on March 12, 2020.[4] As of March 29, 2020, more than 634,000 cases of COVID-19 have been confirmed around the world, resulting in 29,891 deaths.[5] The estimated basic reproduction number (R_0) of COVID-19 is approximately 2.2, meaning that, on average, each patient spreads infection to 2.2 people.[6] Because no specific drugs or vaccines are yet available for COVID-19, early diagnosis and management are crucial for containing the outbreak.

Coronaviruses (CoVs) cause mild to moderate upper respiratory tract illnesses in both humans and animals.[7] SARS-CoV-2, a betacoronavirus, has a single-positive strand

Received: April 3, 2020
Accepted: April 15, 2020
Published: April 15, 2020

ACS Publications © XXXX American Chemical Society

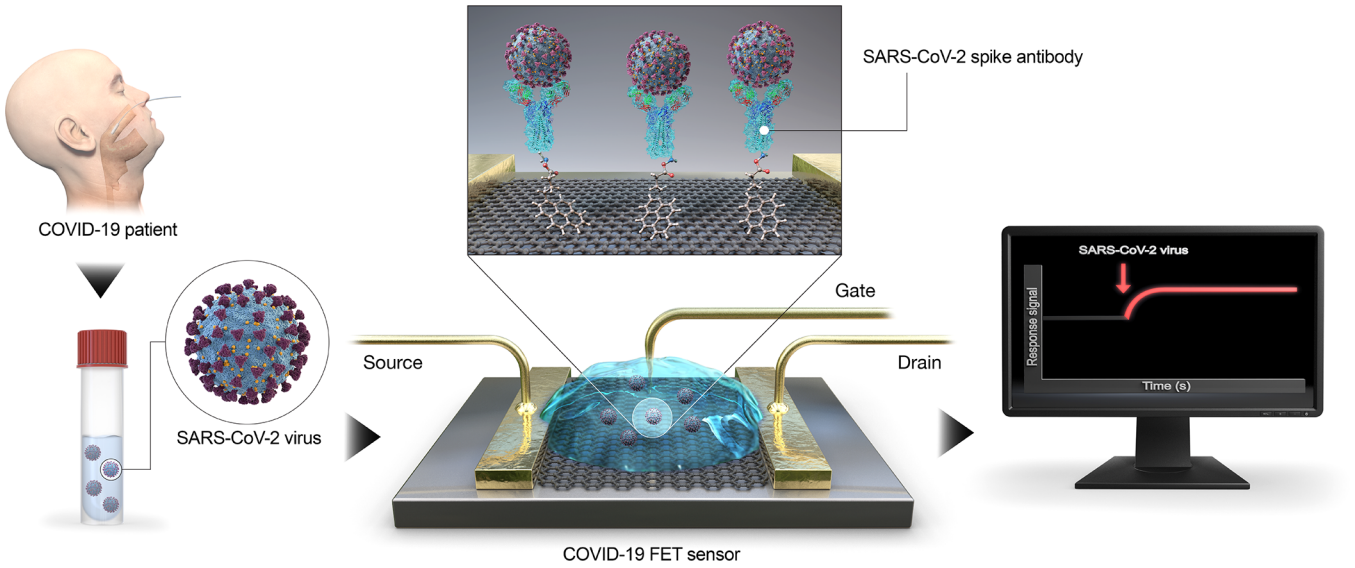

Figure 1. Schematic diagram of COVID-19 FET sensor operation procedure. Graphene as a sensing material is selected, and SARS-CoV-2 spike antibody is conjugated onto the graphene sheet *via* 1-pyrenebutyric acid *N*-hydroxysuccinimide ester, which is an interfacing molecule as a probe linker.

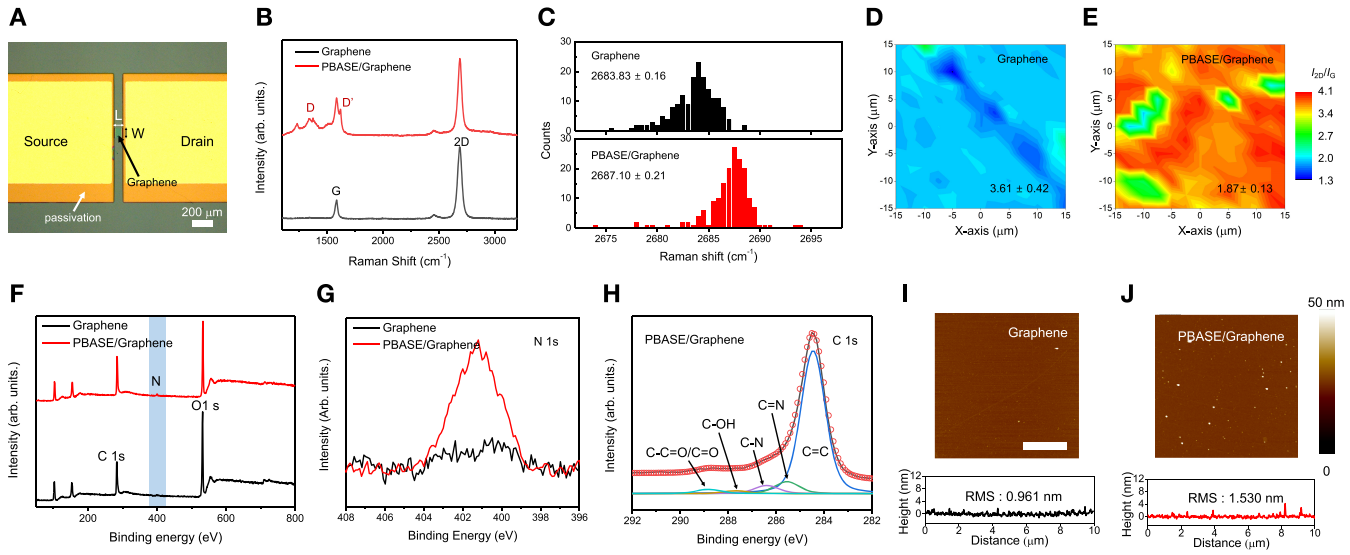

Figure 2. Surface analysis of pristine and PBASE-modified graphene using Raman spectroscopy, X-ray spectroscopy, and atomic force microscopy. (A) Optical image of the COVID-19 FET sensor. The dimensions were 100 × 100 μm^2 ($L \times W$). Scale bar in the image denotes 200 μm. (B) Representative Raman spectra of pristine and PBASE-modified graphene. (C) Comparison of statistical data of the 2D peak position between pristine and PBASE-modified graphene. Mapping images of average I_{2D}/I_G ratio (D) before and (E) after PBASE modification. (F) XPS survey data of pristine and PBASE-modified graphene. (G) N 1s peak of pristine and PBASE-treated graphene (shadow region in F). (H) Deconvoluted C 1s peak of PBASE-modified graphene. Atomic force microscopy (AFM) images of (I) pristine graphene (RMS = 0.961) and (J) PBASE-modified graphene (RMS = 1.530). Bottom graphs indicate the height profiles in the corresponding two AFM images. Scale bar in the image denotes 3 μm.

RNA genome. CoV genomes encode four structural proteins: spike (S), envelope (E), matrix (M), and nucleocapsid (N). Two betacoronaviruses, severe acute respiratory syndrome coronavirus (SARS-CoV) and Middle East respiratory syndrome coronavirus (MERS-CoV), caused serious epidemics over the past two decades.[8] Phylogenetic analysis revealed that SARS-CoV-2 is more similar to SARS-CoV than MERS-CoV.[9] Although the viral pathogenesis of SARS-CoV-2 is unknown, recent studies reported that SARS-CoV-2 uses angiotensin-converting enzyme II (ACE2) as a cellular entry receptor; ACE2 is also a well-known host cell receptor for SARS-CoV.[10] SARS-CoV-2 colocalizes with ACE2 in animal cells,[11] and its spike (S) protein binds ACE2 with high affinity.[12,13]

For emerging pathogens, real-time reverse transcription−polymerase chain reaction (RT-PCR) is the primary means of diagnosis. Currently, real-time RT-PCR is used for the detection of SARS-CoV-2 based on previously published laboratory protocols.[14] SARS-CoV-2 is highly contagious and is currently spreading rapidly around the world; the rate of COVID-19 transmission is much faster than those of SARS and MERS. Moreover, cases of asymptomatic COVID-19 transmission have been reported.[15,16] Molecular diagnosis using real-time RT-PCR takes at least 3 h, including

https://dx.doi.org/10.1021/acsnano.0c02823
ACS Nano XXXX, XXX, XXX−XXX

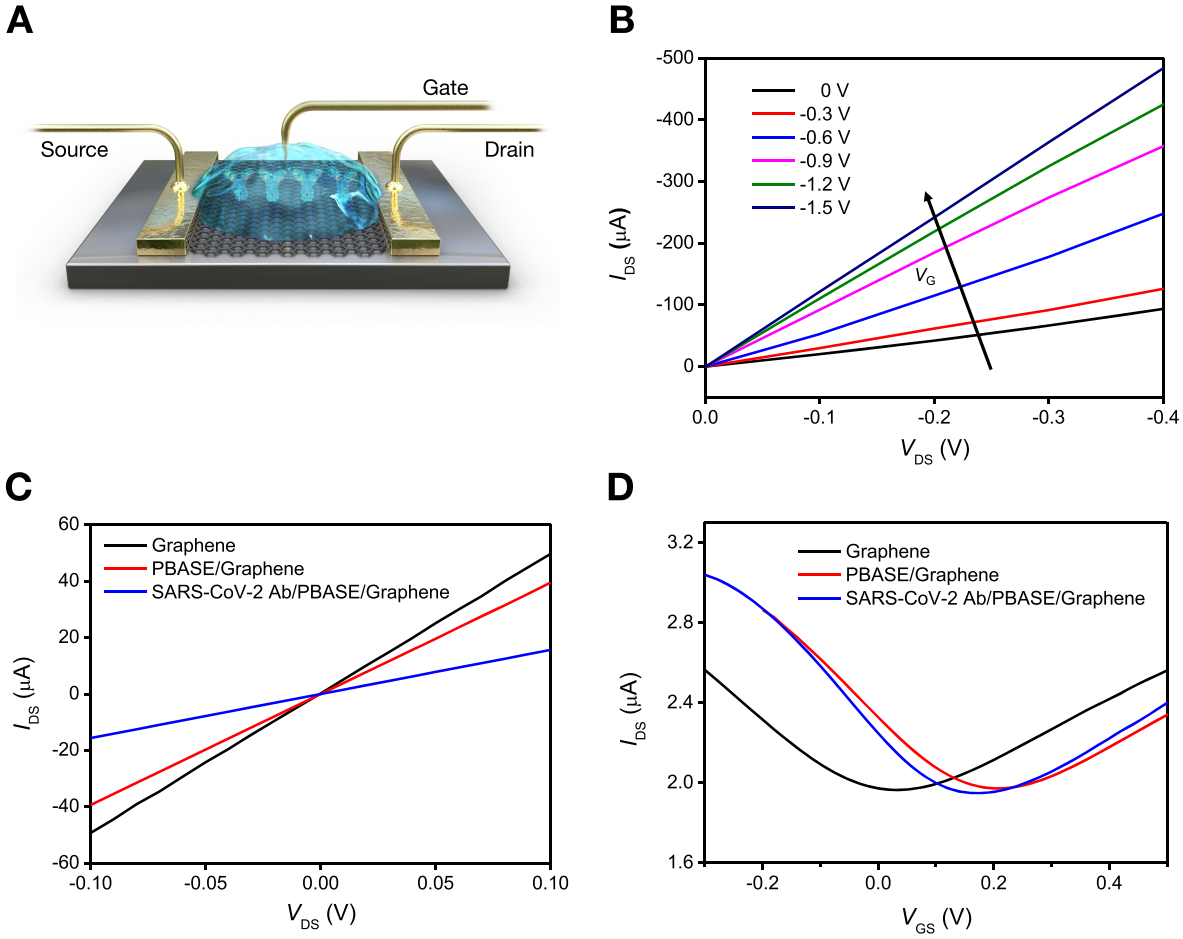

Figure 3. Electrical characterization of pristine, PBASE-modified, and SARS-CoV-2 spike antibody-immobilized graphene. (A) Schematic diagram of the aqueous-solution-gated FET (COVID-19 FET sensor) configuration using the antibody-conjugated graphene. (B) I_{DS}−V_{DS} output curves of the antibody-conjugated FET with various gating voltages from 0 to −1.5 V in steps of −0.3 V. I_{DS} negatively increased as V_{GS} negatively increased. (C) Current−voltage (I−V) characteristics of the graphene-based device of each functionalization process for the antibody modification. (D) Measurement of transfer curves of the COVID-19 FET sensor in steps of the antibody conjugation (V_{DS} = 0.01 V).

preparation of viral RNA. In addition, the RNA preparation step can affect diagnostic accuracy. Hence, highly sensitive immunological diagnostic methods that directly detect viral antigens in clinical samples without sample preparation steps are necessary for rapid and accurate diagnosis of COVID-19.

Among the many diagnostic methods currently available, field-effect transistor (FET)-based biosensing devices have several advantages, including the ability to make highly sensitive and instantaneous measurements using small amounts of analytes.[17,18] FET-based biosensors are considered to be potentially useful in clinical diagnosis, point-of-care testing, and on-site detection. Graphene is a two-dimensional sheet of hexagonally arranged carbon atoms, all of which are exposed on its surface.[19] It has proven to be a useful material for various sensing platforms due to its extraordinary properties, including high electronic conductivity, high carrier mobility, and large specific area.[20] Graphene-based FET biosensors can detect surrounding changes on their surface and provide an optimal sensing environment for ultrasensitive and low-noise detection. From this standpoint, graphene-based FET technology is very attractive for applications related to sensitive immunological diagnosis.[21,22]

In this study, we developed a graphene-based biosensing device functionalized with SARS-CoV-2 spike antibody (COVID-19 FET sensor) for use as a SARS-CoV-2 virus detection platform. SARS-CoV-2 spike antibody was immobilized onto the fabricated device through 1-pyrenebutyric acid N-hydroxysuccinimide ester (PBASE), an efficient interface coupling agent used as a probe linker (Figure 1). Our COVID-19 FET sensor detects target SARS-CoV-2 antigen protein with a limit of detection (LOD) of 1 fg/mL. Most critical of all, we confirmed the potential for clinical application by detecting SARS-CoV-2 antigen protein in transport medium used for nasopharyngeal swabs and cultured SARS-CoV-2 virus, as well as SARS-CoV-2 virus from clinical samples. Furthermore, our sensor could distinguish the SARS-CoV-2 antigen protein from those of MERS-CoV. These results demonstrate the successful fabrication of a COVID-19 FET sensor based on integration of SARS-CoV-2 spike antibody with graphene, enabling highly sensitive detection of the SARS-CoV-2 virus in clinical samples.

RESULTS AND DISCUSSION

Fabrication and Characterization of Biosensing Device. Figure 2A depicts the optical image of the COVID-19 FET sensor. The dimensions of the sensing area were 100 × 100 μm^2 ($L \times W$). To reduce interference during electrical measurements, the device was passivated with SU8-2010.

https://dx.doi.org/10.1021/acsnano.0c02823
ACS Nano XXXX, XXX, XXX−XXX

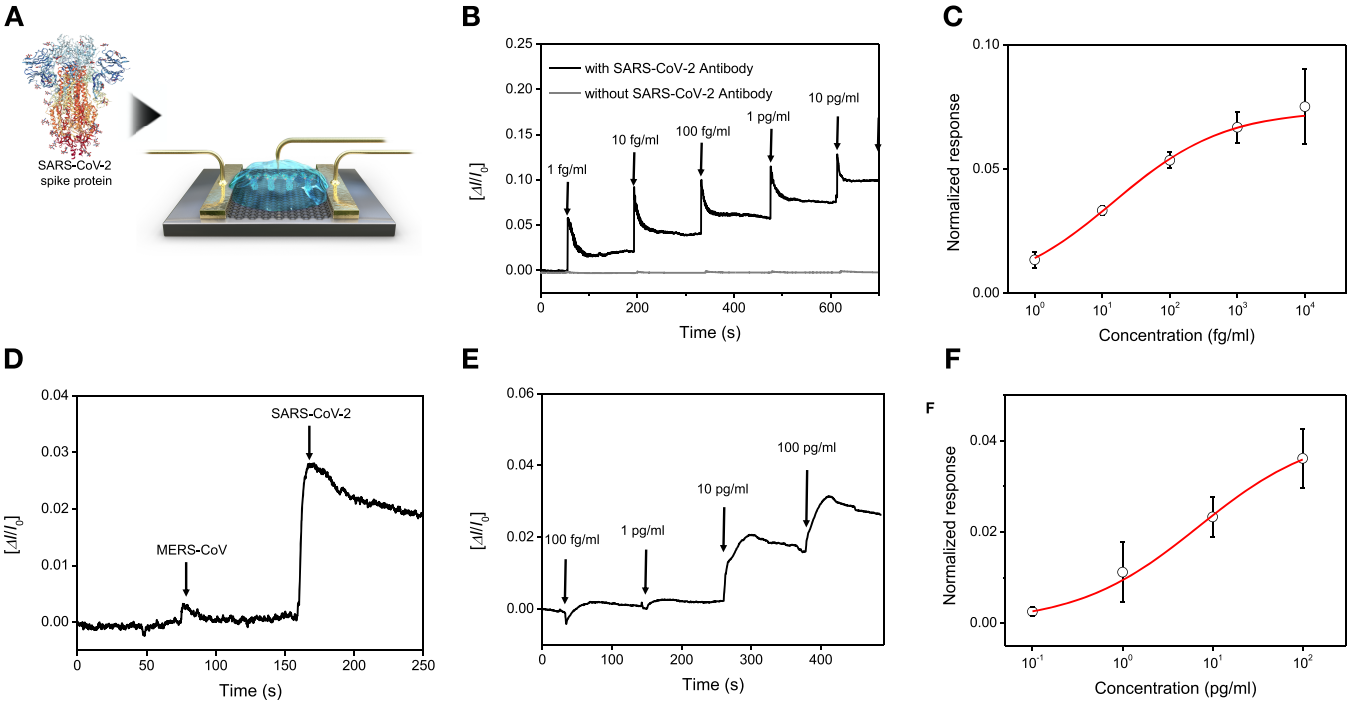

Figure 4. Detection of SARS-CoV-2 antigen protein. (A) Schematic diagram for the COVID-19 FET sensor for detection of SARS-CoV-2 spike protein. (B) Real-time response of COVID-19 FET toward SARS-CoV-2 antigen protein in PBS and (C) related dose-dependent response curve (V_{DS} = 0.01 V). Graphene-based FET without SARS-CoV-2 antibody is presented as negative control. (D) Selective response of COVID-19 FET sensor toward target SARS-CoV-2 antigen protein and MERS-CoV protein. (E) Real-time response of COVID-19 FET toward SARS-CoV-2 antigen protein in UTM and (F) related dose-dependent response curve.

Details of the fabrication of the COVID-19 FET sensor is provided in Materials and Methods. To confirm that the graphene surface was chemically functionalized using PBASE, we obtained Raman spectra and X-ray photoelectron spectroscopy (XPS) data (Figure 2B−H). Figure 2B shows the Raman spectra of the pristine and PBASE-modified graphene surfaces. In the spectrum for the surface of pristine graphene, two major peaks (the G and 2D peaks) were observed. The G peak corresponds to the lattice vibration mode, and the 2D peak stems from second-order Raman scattering. However, the D and D′ peaks obviously appeared due to the relative resonance of sp^3 bonding, orbital hybridization, and a pyrene group in the binding of PABSE to the graphene surface. To provide a visual comparison of the qualities of graphene after modification with PBASE, we converted the measured data to histograms and mapping images (Figure 2C−E). After PBASE was applied to the graphene surface, the statistical data of the 2D peak position were shifted to a higher frequency (∼3.27 cm^{-1}), indicating p-doping by the $\pi-\pi$ interaction between PBASE and graphene (Figure 2C).[23,24] The mapping images also show that the average I_{2D}/I_G ratio of PBASE-treated graphene (I_{2D}/I_G = ∼1.87) is significantly lower than that of pristine graphene (I_{2D}/I_G = ∼3.61) due to existence of some disorder on the graphene (Figure 2D,E).

The XPS survey data show the principal C 1s, O 1s, and N 1s core levels (Figure 2F). Before functionalization, the graphene exhibited no meaningful N peak (black line), whereas the N 1s peak was observed in the PBASE-treated sample (red line). Figure 2G indicates the comparison of the N 1s peak intensity before and after PBASE functionalization. The increase in intensity of the N 1s peak suggests successful surface modification. The C 1s peak was composed of five components, 284.5, 285.5, 286.4, 287.7, and 288.6 eV, corresponding to C═C, C═N, C−N, C−OH, and C−C═O/C═O, respectively, originating from the substitutional doping of N atoms (Figure 2H).[25] These results suggest that the surface of PBASE-modified graphene can be successfully used as a substrate support for stable sensing.

Next, we characterized the morphology and quality of the graphene sheets using atomic force microscopy (AFM) and high-resolution transmission electron microscopy (HR-TEM). The surface roughness of graphene (RMS) increased slightly from ∼0.961 nm to ∼1.530 nm after PBASE modification (Figure 2I,J). The general profile of the graphene sheet and its electron diffraction pattern of the sheets reveal the fine crystallinity of the graphene on the EM grid (Figure S1).

Selection of the Antigen and Validation of the Antibody. SARS-CoV-2 encodes four structural proteins: spike, envelope, matrix, and nucleocapsid.[9] Among them, the spike protein is best suited for use as a diagnostic antigen because it is a major transmembrane protein of the virus and is highly immunogenic. In addition, the spike protein exhibits amino acid sequence diversity among coronaviruses,[9] enabling the specific detection of SARS-CoV-2. Therefore, we used SARS-CoV-2 spike antibody as a receptor to detect this virus.

Before immobilizing SARS-CoV-2 spike antibody onto the FET, we verified the performance of the antibody by enzyme-linked immunosorbent assay (ELISA). The results revealed that the antibody bound to the SARS-CoV-2 spike protein but not to the MERS-CoV spike protein or bovine serum albumin (BSA) (Figure S2). These observations confirm that the antibody is specific for the SARS-CoV-2 spike protein and is therefore suitable for detecting SARS-CoV-2. The detection limit of the antibody in the ELISA platform was 4 ng/mL.

Preparation of the COVID-19 FET Sensor. To evaluate the presence of the SARS-CoV-2 spike antibody on the

https://dx.doi.org/10.1021/acsnano.0c02823
ACS Nano XXXX, XXX, XXX−XXX

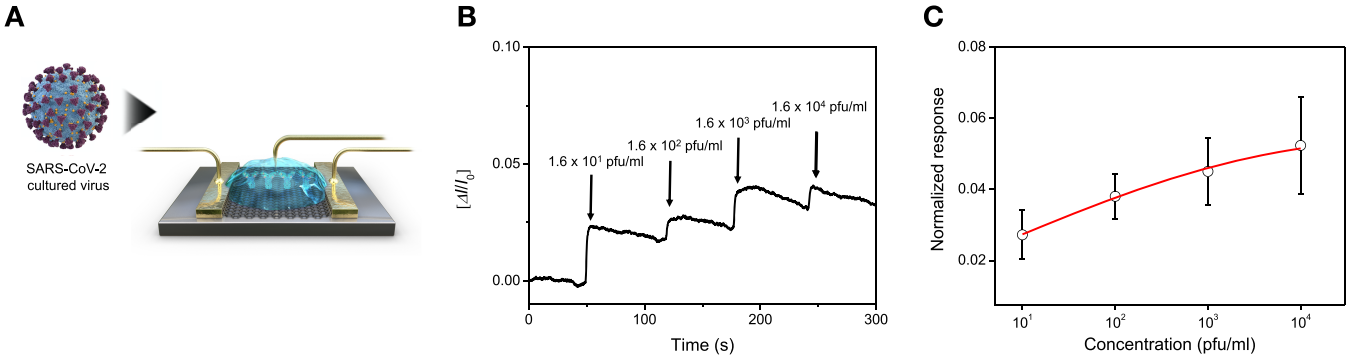

Figure 5. Detection of cultured SARS-CoV-2 virus. (A) Schematic diagram for the COVID-19 FET sensor for detection of SARS-CoV-2 cultured virus. (B) Real-time response of COVID-19 FET toward SARS-CoV-2 cultured virus and (C) related dose-dependent response curve.

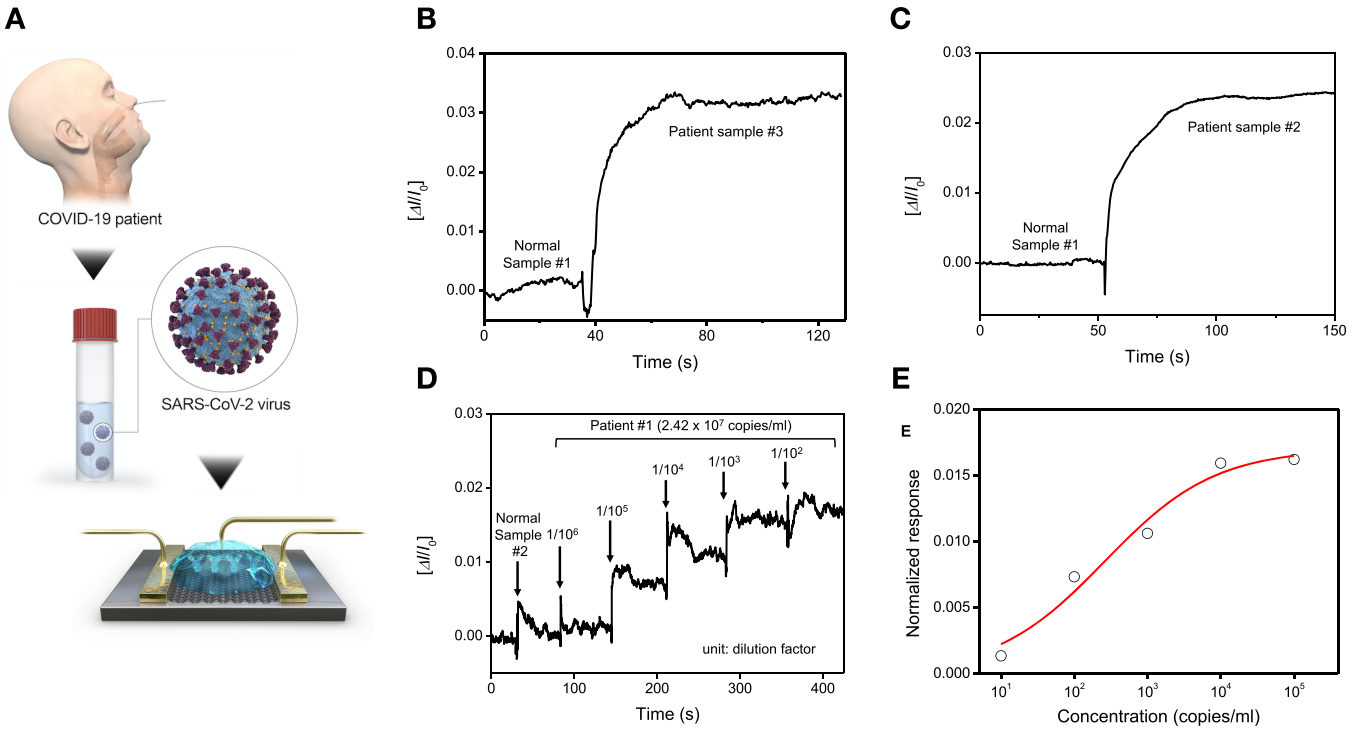

Figure 6. Detection of SARS-CoV-2 virus from clinical samples. (A) Schematic diagram for the COVID-19 FET sensor for detection of SARS-CoV-2 virus from COVID-19 patients. (B,C) Comparison of response signal between normal samples and patient ones. (D) Real-time response of COVID-19 FET toward SARS-CoV-2 clinical sample and (C) related dose-dependent response curve.

graphene surface, we carried out electrical measurements. Figure 3C shows the current−voltage (I−V) curves of the graphene device over a range from −0.1 to +0.1 V before and after attachment of the antibody. After PBASE functionalization and immobilization of the antibody onto the graphene channel, the slopes (dI/dV) decreased. This difference in slope indicates the successful introduction of the SARS-CoV-2 spike antibody.

To investigate the possibility of transducing an electrical signal with the COVID-19 FET sensor, we prepared an aqueous solution-gated FET. The geometry of the COVID-19 FET sensor was designed using a graphene channel conjugated to the SARS-CoV-2 spike antibody, and the FET was covered with phosphate-buffered saline (PBS; pH 7.4) buffer as the electrolyte to maintain an efficient gating effect. As shown in Figure 3A, the aqueous solution-gated FET system could detect SARS-CoV-2 based on changes in channel surface potential and the corresponding effects on the electrical response.

We measured the transfer curves of the graphene-based FET after each modification process (Figure 3D). After PBASE functionalization, an obvious positive shift was observed due to the p-doping effect of the pyrene group. However, the transfer curve was shifted negatively, suggesting that the positive charge of the antibody exerted an n-doping effect on graphene after the antibody was immobilized. Figure 3B shows the output curves of the COVID-19 FET sensor as a function of gate voltage (V_G) over a range from 0 to −1.5 V in steps of −0.3 V. I_{DS} negatively increased as V_G negatively increased, corresponding to the predicted behavior of a p-type semiconductor.[26,27] Moreover, the linear I−V curves exhibited highly stable ohmic contact, indicating that the COVID-19 FET sensor provided a reliable electrical signal for detection of the target analytes (SARS-CoV-2 antigen protein, cultured

https://dx.doi.org/10.1021/acsnano.0c02823
ACS Nano XXXX, XXX, XXX−XXX

SARS-CoV-2 virus, or SARS-CoV-2 virus from clinical samples).

Real-Time Detection of SARS-CoV-2 Antigen Protein. To investigate the performance of the COVID-19 FET sensor, we evaluated the dynamic response of the sensor to spike protein (Figure 4A). First, we measured the sensor's LOD for spike protein. The sensor responded to 1 fg/mL of SARS-CoV-2 spike protein in PBS (Figure 4B); that is, the LOD of the FET sensor was substantially lower than that of the ELISA platform (Figure S2). However, the pristine graphene-based device without SARS-CoV-2 spike protein conjugation did not show any remarkable signal change after the introduction of various sample concentrations (gray line in Figure 4D). The control experiment indicates that the SARS-CoV-2 spike protein is essential for specific binding with the SARS-CoV-2 antigen. In addition, the COVID-19 FET sensor exhibited no response to MERS-CoV spike proteins (Figure 4D), indicating that the COVID-19 FET sensor was both highly sensitive and specific for the SARS-CoV-2 spike antigen protein.

In the clinic, diagnosis of COVID-19 is performed using nasopharyngeal swabs suspended in universal transport medium (UTM). The UTM contains various reagents that may affect performance of the FET sensor, such as Hank's balanced salts and BSA. Therefore, we assessed the response of the FET sensor to antigens in UTM. To determine whether the FET sensor could be used in the field, we measured the response of the FET sensor to SARS-CoV-2 spike proteins in 0.01× UTM. The results revealed that the FET sensor could successfully detect SARS-CoV-2 spike antigen proteins starting from a concentration of 100 fg/mL (Figure 4E). This indicates that the COVID-19 FET sensor can detect antigens in clinical samples without any preparation or preprocessing. To further investigate the normalized sensitivity of the COVID-19 FET sensor, the changes in sensitivity as a function of SARS-CoV-2 antigen protein concentration were characterized by fitting each data point, as shown in Figure 4C,F.

Real-Time Detection of Cultured SARS-CoV-2 Virus. Next, we investigated whether the COVID-19 FET sensor could detect SARS-CoV-2 virus (Figure 5A). To this end, we propagated SARS-CoV-2 in cultured cells and inactivated viral infectivity by heating. Upon application of cultured SARS-CoV-2, the COVID-19 FET sensor responded to concentrations as low as 1.6×10^1 pfu/mL (Figure 5B), and the normalized response curve was linear from 1.6×10^1 to 1.6×10^4 pfu/mL (Figure 5C). This result suggests that the COVID-19 FET sensor has the potential to be used for COVID-19 diagnosis.

Detection of SARS-CoV-2 Virus from Clinical Samples. Finally, we tested the detection performance of the COVID-19 FET sensor using clinical samples (Figure 6A). To this end, we collected nasopharyngeal swab specimens from COVID-19 patients and normal subjects and stored them in UTM. Prior to addition of patient samples to the device, we evaluated nasopharyngeal swab samples from normal subjects to determine the basal signal. The COVID-19 FET sensor clearly discriminated between patient and normal samples (Figure 6B,C). In addition, the FET sensor responded to patient samples diluted as much as $1{:}1 \times 10^5$ (242 copies/mL) (Figure 6D), and the normalized response curve of the FET sensor was linear (Figure 6E). Given that UTM includes various reagents and generates noise signals, we consider the LOD of the COVID-19 FET sensor to be low enough for practical use Table S2. Nevertheless, development of novel materials of the FET sensor for UTM should be necessary for more accurate detection by reducing the noise signals. For reference, the detection limit of current molecular diagnostic tests of COVID-19 is ∼50−100 copies.[28] Taken together, our findings show that our COVID-19 FET sensor successfully detected SARS-CoV-2 virus from clinical samples without any preprocessing and with a large dynamic range.

CONCLUSION

During the COVID-19 pandemic, the development of highly sensitive and rapid biosensing devices has become increasingly important. We developed a COVID-19 FET sensor in which the SARS-CoV-2 spike antibody is conjugated to a graphene sheet, which is used as the sensing area. The sensor was able to detect SARS-CoV-2 virus in clinical samples, the SARS-CoV-2 antigen in practical use (Table S2). standard buffer, transport medium,, and cultured SARS-CoV-2 virus. Furthermore, the device exhibited no measurable cross-reactivity with MERS-CoV antigen. Therefore, our functionalized graphene-based sensor platform provides simple, rapid, and highly responsive detection of the SARS-CoV-2 virus in clinical samples. Moreover, this technology could be adapted for diagnosis of other emerging viral diseases.

MATERIALS AND METHODS

Fabrication of Graphene-Based Sensing Devices. Graphene was transferred to a SiO_2/Si substrate using conventional wet-transfer methods. Poly(methyl methacrylate) (PMMA) C4 (MicroChem, Newton, MA) was spin-coated at 500 rpm for 10 s and at 3000 rpm for 30 s onto graphene on Cu foil (Grolltex, San Diego, CA). PMMA/graphene on Cu foil was etched in CE-100 copper etchant (Transene, Oakland, CA). After the Cu foil was etched, the PMMA/graphene layers were moved using clean glass slides into a deionized (DI) water bath, and the copper etchant was washed away. Subsequently, the PMMA/graphene layer was transferred to a SiO_2/Si substrate and dried under ambient conditions overnight. The PMMA layer was removed in an acetone bath for 2 h. Finally, the graphene was transferred onto the substrate, followed by isopropyl alcohol washing and drying under a stream of N_2 gas.

To fabricate practical graphene-based devices, the transferred graphene was patterned into linear shapes by photolithography and etched by a reactive ion-etching method. To generate a Au/Cr electrode layer on the etched graphene layer, metallization was performed using a thermal evaporation method and a lift-off technique. The device dimensions were $100 \times 100\ \mu m^2$ ($L \times W$). To reduce interference during electrical measurements, the device was passivated with SU8-2010 (MicroChem).

Immobilization of SARS-CoV-2 Antibody on the Graphene Surface. The fabricated graphene-based device was soaked in 2 mM PBASE (Thermo Fisher Scientific, Waltham, MA) in methanol for 1 h at room temperature and then rinsed several times with PBS and DI water. Finally, the functionalized device was exposed to 250 μg/mL SARS-CoV-2 spike antibody for 4 h.

Instruments. Pristine graphene and graphene with PBASE modification were characterized by Raman spectroscopy, XPS, AFM, and HR-TEM.

Raman spectrum and mapping analysis was acquired with an inVia Raman system (Renishaw, UK). Mapping images were obtained from 196 spectra ($30 \times 30\ \mu m$ area on graphene). The intervals between adjacent spectrum points were 2.5 μm (horizontal and vertical). Analysis of the chemical binding component was determined by XPS on a K-Alpha instrument (Thermo Fisher Scientific), with the incident beam produced by an Al X-ray source ($h\nu$ = 1486.6 eV) and a pass energy of 50 eV. Surface roughness analysis was conducted by AFM on a Dimension 3000 instrument (Digital Instruments/Veeco Science). HR-TEM imaging was performed on a ZEISS Libra

https://dx.doi.org/10.1021/acsnano.0c02823
ACS Nano XXXX, XXX, XXX−XXX

ultracorrected energy filtering transmission electron microscope (ZEISS, Germany) with a 200 kV acceleration voltage.

Sensing Measurement. Electrical performance was evaluated on a 2634B semiconductor analyzer (Keithley Instruments, Cleveland, OH) and probe station. A drain−source bias voltage of ∼10 mV was maintained during measurement. The detected electrical response signal was normalized as $[\Delta I/I_0] = (I - I_0)/I_0$, where I is the detected real-time current and I_0 is the initial current.

Enzyme-Linked Immunosorbent Assay. A 96-well plate was coated with SARS-CoV-2 spike antigen protein (40591-V08H; Sino Biological, Inc., China) or MERS-CoV spike antigen protein (40069-V08H, Sino Biological) for 1 h at 37 °C and then blocked with 5% BSA. A proper dilution of SARS-CoV-2 spike antibody (40150-R007, Sino Biological) was added to the blocked well, and the sample was incubated for 1 h at room temperature. After being washed with TBST (Tris-buffered saline, 0.1% Tween 20), horseradish peroxidase-conjugated anti-rabbit IgG antibody (#7074, Cell Signaling Technology, Danvers, MA) was added, and the sample was incubated for 1 h at room temperature. After extensive washing with TBST, the ELISA substrate (1-Step Ultra TMB-ELISA, Thermo Fisher Scientific) was applied, and signals were obtained on a Synergy HTX plate reader (BioTek Instruments, Winooski, VT).

Virus Culture. Virus infection experiments were performed in a biosafety level 3 laboratory. African green monkey kidney Vero E6 cells were infected with a clinical isolate of SARS-CoV-2 (BetaCoV/Korea/KCDC03/2020, provided by Korea CDC). After 48 h, the culture medium containing mature infectious virions (virus medium) was collected, and viral titer was determined by plaque assay. Live virus was inactivated by heating at 100 °C for 15 min and was stored at −80 °C for further use.

Clinical Sample Preparation. The clinical samples used in this study (Figure S3 and Table S1) were collected from subjects as part of registered protocols approved by Institutional Review Board (IRB) of Jeonbuk National University Hospital, and all patients provided written informed consent (IRB registration number: CUH 2020-02-050-008). Nasopharyngeal swabs from COVID-19 patients and healthy subjects were stored in UTM (Noble Biosciences, South Korea). Viral copy number was determined by real-time RT-PCR. Clinical samples were inactivated by heating at 100 °C for 10 min and were stored at −80 °C for further use.

ASSOCIATED CONTENT

Supporting Information

The Supporting Information is available free of charge at https://pubs.acs.org/doi/10.1021/acsnano.0c02823.

Figures of TEM observation of the graphene sheet, ELISA details, clinical sample information on COVID-19 patients, and performance comparison on SARS-CoV-2 detection technologies (PDF)

AUTHOR INFORMATION

Corresponding Authors

Edmond Changkyun Park − *Research Center for Bioconvergence Analysis, Korea Basic Science Institute, Cheongju 28119, Republic of Korea; Center for Convergent Research of Emerging Virus Infection, Korea Research Institute of Chemical Technology, Daejeon 34114, Republic of Korea; Department of Bio-Analysis Science, University of Science & Technology (UST), Daejeon 34113, Republic of Korea;* orcid.org/0000-0001-6699-4886; Email: edpark@kbsi.re.kr

Seung Il Kim − *Research Center for Bioconvergence Analysis, Korea Basic Science Institute, Cheongju 28119, Republic of Korea; Center for Convergent Research of Emerging Virus Infection, Korea Research Institute of Chemical Technology, Daejeon 34114, Republic of Korea; Department of Bio-Analysis Science, University of Science & Technology (UST), Daejeon 34113, Republic of Korea;* orcid.org/0000-0001-6681-4486; Email: ksi@kbsi.re.kr

Authors

Giwan Seo − *Research Center for Bioconvergence Analysis, Korea Basic Science Institute, Cheongju 28119, Republic of Korea; Center for Convergent Research of Emerging Virus Infection, Korea Research Institute of Chemical Technology, Daejeon 34114, Republic of Korea;* orcid.org/0000-0002-8734-6199

Geonhee Lee − *Advanced Materials Division, Korea Research Institute of Chemical Technology, Daejeon 34114, Republic of Korea*

Mi Jeong Kim − *Research Center for Bioconvergence Analysis, Korea Basic Science Institute, Cheongju 28119, Republic of Korea; Center for Convergent Research of Emerging Virus Infection, Korea Research Institute of Chemical Technology, Daejeon 34114, Republic of Korea*

Seung-Hwa Baek − *Center for Convergent Research of Emerging Virus Infection, Korea Research Institute of Chemical Technology, Daejeon 34114, Republic of Korea; Department of Predictive Toxicology, Korea Institute of Toxicology, Daejeon 34114, Republic of Korea*

Minsuk Choi − *Center for Convergent Research of Emerging Virus Infection, Korea Research Institute of Chemical Technology, Daejeon 34114, Republic of Korea*

Keun Bon Ku − *Center for Convergent Research of Emerging Virus Infection, Korea Research Institute of Chemical Technology, Daejeon 34114, Republic of Korea*

Chang-Seop Lee − *Department of Internal Medicine, Jeonbuk National University Medical School, Jeonju 54986, Republic of Korea; Biomedical Research Institute of Jeonbuk National University Hospital, Jeonju 54907, Republic of Korea*

Sangmi Jun − *Center for Convergent Research of Emerging Virus Infection, Korea Research Institute of Chemical Technology, Daejeon 34114, Republic of Korea; Center for Research Equipment, Korea Basic Science Institute, Cheongju 28119, Republic of Korea*

Daeui Park − *Center for Convergent Research of Emerging Virus Infection, Korea Research Institute of Chemical Technology, Daejeon 34114, Republic of Korea; Department of Predictive Toxicology, Korea Institute of Toxicology, Daejeon 34114, Republic of Korea;* orcid.org/0000-0002-9452-5849

Hong Gi Kim − *Center for Convergent Research of Emerging Virus Infection, Korea Research Institute of Chemical Technology, Daejeon 34114, Republic of Korea*

Seong-Jun Kim − *Center for Convergent Research of Emerging Virus Infection, Korea Research Institute of Chemical Technology, Daejeon 34114, Republic of Korea*

Jeong-O Lee − *Advanced Materials Division, Korea Research Institute of Chemical Technology, Daejeon 34114, Republic of Korea;* orcid.org/0000-0002-7343-4892

Bum Tae Kim − *Center for Convergent Research of Emerging Virus Infection, Korea Research Institute of Chemical Technology, Daejeon 34114, Republic of Korea*

Complete contact information is available at: https://pubs.acs.org/10.1021/acsnano.0c02823

Notes

The authors declare no competing financial interest.

https://dx.doi.org/10.1021/acsnano.0c02823
ACS Nano XXXX, XXX, XXX−XXX

ACKNOWLEDGMENTS

This work was supported by National Research Council of Science and Technology (NST) funded by the Ministry of Science and ICT, Republic of Korea (Grant No. CRC-16-01-KRICT), and Korea Health Technology R&D Project through the Korea Health Industry Development Institute (KHIDI), funded by the Ministry of Health & Welfare, Republic of Korea (Grant Nos. HI20C0033 and HI20C0363).

REFERENCES

(1) WHO. Novel Coronavirus (2019-nCoV) Situation Report − 1. https://www.who.int/docs/default-source/coronaviruse/situation-reports/20200121-sitrep-1-2019-ncov.pdf?sfvrsn=20a99c10_4 (accessed 2020-04-15).

(2) Wu, F.; Zhao, S.; Yu, B.; Chen, Y. M.; Wang, W.; Song, Z. G.; Hu, Y.; Tao, Z. W.; Tian, J. H.; Pei, Y. Y.; Yuan, M. L.; Zhang, Y. L.; Dai, F. H.; Liu, Y.; Wang, Q. M.; Zheng, J. J.; Xu, L.; Holmes, E. C.; Zhang, Y. Z. A New Coronavirus Associated with Human Respiratory Disease in China. *Nature* **2020**, *579*, 265−269.

(3) Coronaviridae Study Group of the International Committee on Taxonomy of Viruses.. The Species Severe Acute Respiratory Syndrome-Related Coronavirus: Classifying 2019-nCoV and Naming It SARS-CoV-2. *Nat. Microbiol.* **2020**, *5*, 536−544.

(4) WHO. Coronavirus Disease 2019 (COVID-19): Situation Report − 52. https://www.who.int/docs/default-source/coronaviruse/situation-reports/20200312-sitrep-52-covid-19.pdf?sfvrsn=e2bfc9c0_4 (accessed 2020-04-15).

(5) WHO. Coronavirus Disease 2019 (COVID-19): Situation Report − 69. https://www.who.int/docs/default-source/coronaviruse/situation-reports/20200329-sitrep-69-covid-19.pdf?sfvrsn=8d6620fa_4 (accessed 2020-04-15).

(6) Li, Q.; Guan, X.; Wu, P.; Wang, X.; Zhou, L.; Tong, Y.; Ren, R.; Leung, K. S. M.; Lau, E. H. Y.; Wong, J. Y.; Xing, X.; Xiang, N.; Wu, Y.; Li, C.; Chen, Q.; Li, D.; Liu, T.; Zhao, J.; Liu, M.; Tu, W.; et al. Early Transmission Dynamics in Wuhan, China, of Novel Coronavirus-Infected Pneumonia. *N. Engl. J. Med.* **2020**, *382*, 1199−1207.

(7) Li, G.; Fan, Y.; Lai, Y.; Han, T.; Li, Z.; Zhou, P.; Pan, P.; Wang, W.; Hu, D.; Liu, X.; Zhang, Q.; Wu, J. Coronavirus Infections and Immune Responses. *J. Med. Virol.* **2020**, *92*, 424−432.

(8) de Wit, E.; van Doremalen, N.; Falzarano, D.; Munster, V. J. SARS and MERS: Recent Insights into Emerging Coronaviruses. *Nat. Rev. Microbiol.* **2016**, *14*, 523−534.

(9) Lu, R.; Zhao, X.; Li, J.; Niu, P.; Yang, B.; Wu, H.; Wang, W.; Song, H.; Huang, B.; Zhu, N.; Bi, Y.; Ma, X.; Zhan, F.; Wang, L.; Hu, T.; Zhou, H.; Hu, Z.; Zhou, W.; Zhao, L.; Chen, J.; et al. Genomic Characterisation and Epidemiology of 2019 Novel Coronavirus: Implications for Virus Origins and Receptor Binding. *Lancet* **2020**, *395*, 565−574.

(10) Li, W.; Moore, M. J.; Vasilieva, N.; Sui, J.; Wong, S. K.; Berne, M. A.; Somasundaran, M.; Sullivan, J. L.; Luzuriaga, K.; Greenough, T. C.; Choe, H.; Farzan, M. Angiotensin-Converting Enzyme 2 Is a Functional Receptor for the SARS Coronavirus. *Nature* **2003**, *426*, 450−454.

(11) Zhou, P.; Yang, X. L.; Wang, X. G.; Hu, B.; Zhang, L.; Zhang, W.; Si, H. R.; Zhu, Y.; Li, B.; Huang, C. L.; Chen, H. D.; Chen, J.; Luo, Y.; Guo, H.; Jiang, R. D.; Liu, M. Q.; Chen, Y.; Shen, X. R.; Wang, X.; Zheng, X. S.; et al. A Pneumonia Outbreak Associated with a New Coronavirus of Probable Bat Origin. *Nature* **2020**, *579*, 270−273.

(12) Tian, X.; Li, C.; Huang, A.; Xia, S.; Lu, S.; Shi, Z.; Lu, L.; Jiang, S.; Yang, Z.; Wu, Y.; Ying, T. Potent Binding of 2019 Novel Coronavirus Spike Protein by a SARS Coronavirus-Specific Human Monoclonal Antibody. *Emerging Microbes Infect.* **2020**, *9*, 382−385.

(13) Wrapp, D.; Wang, N.; Corbett, K. S.; Goldsmith, J. A.; Hsieh, C. L.; Abiona, O.; Graham, B. S.; McLellan, J. S. Cryo-EM Structure of the 2019-nCoV Spike in the Prefusion Conformation. *Science* **2020**, *367*, 1260−1263.

(14) WHO. Coronavirus Disease (COVID-19) Technical Guidance: Laboratory Testing for 2019-nCoV in Humans. https://www.who.int/emergencies/diseases/novel-coronavirus-2019/technical-guidance/laboratory-guidance (accessed 2020-04-15).

(15) Bai, Y.; Yao, L.; Wei, T.; Tian, F.; Jin, D. Y.; Chen, L.; Wang, M. Presumed Asymptomatic Carrier Transmission of COVID-19. *JAMA* **2020**, *323*, 1406−1407.

(16) Zou, L.; Ruan, F.; Huang, M.; Liang, L.; Huang, H.; Hong, Z.; Yu, J.; Kang, M.; Song, Y.; Xia, J.; Guo, Q.; Song, T.; He, J.; Yen, H. L.; Peiris, M.; Wu, J. SARS-CoV-2 Viral Load in Upper Respiratory Specimens of Infected Patients. *N. Engl. J. Med.* **2020**, *382*, 1177−1179.

(17) Janissen, R.; Sahoo, P. K.; Santos, C. A.; da Silva, A. M.; von Zuben, A. A. G.; Souto, D. E. P.; Costa, A. D. T.; Celedon, P.; Zanchin, N. I. T.; Almeida, D. B.; Oliveira, D. S.; Kubota, L. T.; Cesar, C. L.; Souza, A. P.; Cotta, M. A. InP Nanowire Biosensor with Tailored Biofunctionalization: Ultrasensitive and Highly Selective Disease Biomarker Detection. *Nano Lett.* **2017**, *17*, 5938−5949.

(18) Liu, J.; Chen, X.; Wang, Q.; Xiao, M.; Zhong, D.; Sun, W.; Zhang, G.; Zhang, Z. Ultrasensitive Monolayer MoS_2 Field-Effect Transistor Based DNA Sensors for Screening of Down Syndrome. *Nano Lett.* **2019**, *19*, 1437−1444.

(19) Cooper, D. R.; D'Anjou, B.; Ghattamaneni, N.; Harack, B.; Hilke, M.; Horth, A.; Majlis, N.; Massicotte, M.; Vandsburger, L.; Whiteway, E.; Yu, V. Experimental Review of Graphene. *ISRN Condens. Matter Phys.* **2012**, *2012*, 501686.

(20) Geim, A. K.; Novoselov, K. S. The Rise of Graphene. *Nat. Mater.* **2007**, *6*, 183−191.

(21) Lei, Y. M.; Xiao, M. M.; Li, Y. T.; Xu, L.; Zhang, H.; Zhang, Z. Y.; Zhang, G. J. Detection of Heart Failure-Related Biomarker in Whole Blood with Graphene Field Effect Transistor Biosensor. *Biosens. Bioelectron.* **2017**, *91*, 1−7.

(22) Zhou, L.; Mao, H.; Wu, C.; Tang, L.; Wu, Z.; Sun, H.; Zhang, H.; Zhou, H.; Jia, C.; Jin, Q.; Chen, X.; Zhao, J. Label-Free Graphene Biosensor Targeting Cancer Molecules Based on Non-Covalent Modification. *Biosens. Bioelectron.* **2017**, *87*, 701−707.

(23) Wu, G.; Tang, X.; Meyyappan, M.; Lai, K. W. C. Doping Effects of Surface Functionalization on Graphene with Aromatic Molecule and Organic Solvents. *Appl. Surf. Sci.* **2017**, *425*, 713−721.

(24) Liu, Y.; Yuan, L.; Yang, M.; Zheng, Y.; Li, L.; Gao, L.; Nerngchamnong, N.; Nai, C. T.; Sangeeth, C. S.; Feng, Y. P.; Nijhuis, C. A.; Loh, K. P. Giant Enhancement in Vertical Conductivity of Stacked CVD Graphene Sheets by Self-Assembled Molecular Layers. *Nat. Commun.* **2014**, *5*, 5461.

(25) Liu, J.-Y.; Chang, H.-Y.; Truong, Q. D.; Ling, Y.-C. Synthesis of nitrogen-doped graphene by pyrolysis of ionic-liquid-functionalized graphene. *J. Mater. Chem. C* **2013**, *1*, 1713−1716.

(26) Choi, Y.; Kang, J.; Jariwala, D.; Kang, M. S.; Marks, T. J.; Hersam, M. C.; Cho, J. H. Low-Voltage Complementary Electronics from Ion-Gel-Gated Vertical van der Waals Heterostructures. *Adv. Mater.* **2016**, *28*, 3742−3748.

(27) Teng, F.; Hu, K.; Ouyang, W.; Fang, X. Photoelectric Detectors Based on Inorganic *p*-Type Semiconductor Materials. *Adv. Mater.* **2018**, *30*, 1706262.

(28) Jung, Y. J.; Park, G.-S.; Moon, J. H.; Ku, K.; Beak, S.-H.; Kim, S.; Park, E. C.; Park, D.; Lee, J.-H.; Byeon, C. W.; Lee, J. J.; Maeng, J.-S.; Kim, S. J.; Kim, S. I.; Kim, B.-T.; Lee, M. J.; Kim, H. G. Comparative Analysis of Primer-Probe Sets for the Laboratory Confirmation of SARS-CoV-2. *BioRixv* https://doi.org/10.1101/2020.02.25.964775 (accessed 2020-04-15).

https://dx.doi.org/10.1021/acsnano.0c02823
ACS Nano XXXX, XXX, XXX−XXX